JOURNAL OF THERMOPHYSICS AND HEAT TRANSFER
Vol. 10, No. 1, January–March 1996

Oscillatory Convection Due to Combined Buoyancy and Thermocapillarity

Y. Kamotani* and J. Masud†
Case Western Reserve University, Cleveland, Ohio 44106
and
A. Pline‡
NASA Lewis Research Center, Cleveland, Ohio 44135

An experimental study is performed on oscillatory convection due to combined thermocapillarity and buoyancy in open cylindrical containers. The fluid in the containers is heated by a heating rod placed along the centerline of the containers. Various container diameters, ranging from 0.39 to 3.1 cm, are used to change the effect of buoyancy on steady and oscillatory convection. The container aspect ratio (height/radius) ranges from 0.75 to 2 and the heater diameter is 10% of the container diameter in all cases. The test fluids are 1- and 2-cS silicone oils (Prandtl number = 13 and 27 at 25°C). The velocity field is studied by flow visualization, whereas the temperature field is measured by a thermocouple probe and thermography. The onset of oscillations and the oscillation frequency are investigated under various conditions. It is found that the basic flow structure is mainly unicellular and thermocapillarity is important for the oscillations in all of the tests. When thermocapillarity is dominant, the Marangoni number is not sufficient to describe the onset conditions. When buoyancy is not negligible, it tends to squeeze the primary cell by thermal stratification and the dynamic Bond number is the parameter characterizing the transition.

Nomenclature

Ar = aspect ratio, H/R
Bd = dynamic Bond number, $Gr/R\sigma^{4/3}$
D = container diameter
f = frequency of oscillations
f^* = dimensionless frequency, $(\mu Rf/\sigma_T \Delta T)R\sigma^{1/3}$
Gr = Grashof number, $g\beta\Delta TR^3/\nu^2$
g = gravitational acceleration
H = container height
Ma = Marangoni number, $PrR\sigma$
Ma_{cr} = critical Marangoni number
Pr = Prandtl number, ν/α
R = container radius
$R\sigma$ = surface-tension Reynolds number, $\sigma_T TR/\mu\nu$
(r, z) = coordinate system, Fig. 1
T = temperature
T_C = cold wall temperature
T_H = heater temperature
U_{ref} = reference velocity
α = thermal diffusivity
β = coefficient of expansion
ΔT = $T_H - T_C$
ΔT_{cr} = critical temperature difference
μ = dynamic viscosity
ν = kinematic viscosity
ρ = density
σ = surface tension
σ_T = temperature coefficient of surface tension

Received May 17, 1995; revision received Oct. 9, 1995; accepted for publication Oct. 13, 1995.

*Professor, Department of Mechanical and Aerospace Engineering. Associate Fellow AIAA.
†Research Associate, Department of Mechanical and Aerospace Engineering.
‡Aerospace Engineer, Microgravity Fluid Branch, Space Experiment Division.

Introduction

IT is known that thermocapillary flow undergoes a transition from a steady to an oscillatory state under certain conditions. Since the phenomenon is not only interesting scientifically, but also has important implications for materials processing in microgravity, it has been given much attention lately. Many of the past experiments on oscillatory thermocapillary flows have been conducted in the so-called float-zone configuration, in which a liquid column is suspended between two differentially heated cylindrical rods.[1–5] Kamotani et al.[6] and Lee et al.[7] have studied the phenomenon in cylindrical containers. In all of these tests small test cells were employed to minimize the effects of buoyancy and gravity, and thus, to simulate a low-gravity environment. However, it is interesting to study how the phenomenon is influenced by buoyancy because thermocapillarity and buoyancy interact strongly under certain conditions in 1-g tests. Although the oscillation phenomenon has been studied by many investigators, its cause is not yet fully understood, in part because the ground-based experimental data available on the phenomenon are confusing or contradictory, partly due to buoyancy. Therefore, the objective of the present study is to obtain some insight into the effect of buoyancy on oscillatory thermocapillary flow.

Combined steady thermocapillary and buoyant flow in rectangular containers has been investigated both numerically[8,9] and experimentally.[10,11] Oscillatory convection due to combined driving forces has been studied numerically in low aspect ratio (height/length) rectangular containers by Ben Hadid and Roux[12] and Mundrane and Zebib[13] for low Pr fluids, and experimentally by Villers and Platten[14] with acetone ($Pr = 4.2$), in all of which the flow has multicellular structure and becomes oscillatory only in the presence of buoyancy. Lee and Kamotani[15] studied oscillatory convection due to combined driving forces in rectangular enclosures of unit order aspect ratio in which the fluid was heated by a thin wire on the free surface, but the experiment covered only a limited range of buoyancy-to-thermocapillarity ratio.

In the present work oscillatory convection is studied experimentally in cylindrical containers of unit order aspect ratio with high Prandtl number fluids. It is an extension of the work

by Kamotani et al.[6] in which oscillatory thermocapillary flow was investigated. In the present study the parametric ranges are chosen so that both thermocapillarity-dominated situations and combined driving-force (thermocapillarity + buoyancy) situations are covered. The conditions for the onset of oscillations, the oscillation frequencies, and the bulk and surface temperature distributions are measured under various conditions. The experiment is supplemented by numerical analysis of the steady flowfields. This article is based on the report by Masud et al.[16] In the experiment called the oscillatory thermocapillary flow experiment (OTFE), which was conducted aboard the Spacelab in 1992, a configuration very similar to the present one was employed.[17] The results from the OTFE are presented herein for comparison.

Experimental Apparatus, Conditions, and Procedure

Apparatus

The primary purpose of designing the experimental apparatus is to study the effect of buoyancy on steady and oscillatory thermocapillary flow in cylindrical containers. For this purpose test sections of various diameters are used, the smallest being 0.39 cm and the largest being 3.1 cm.

The experimental setup consists of six basic components: 1) the fluid, 2) the test section, 3) the heating system, 4) the cooling system, 5) the temperature measurement system, and 6) the flow visualization system. Silicone oil is placed in the cylindrical container and heated by a heater at the center axis. The test section sidewall is maintained at a constant temperature by a cooling system, which maintains a temperature difference between the heater and the test section sidewall. A 386 personal computer with a data acquisition card is connected to thermocouples via an interface to form the temperature measuring system. For flow visualization, a microscope of variable magnification and a high resolution video system are used. Alpha-alumina micropolish powder of 1-μm size are used as the seeding particles. Figure 1 shows the general layout of the test section.

Silicone oils of 2- and 1-cS kinematic viscosity are chosen as the test fluids. The surface tension of this fluid is known to be insensitive to surface contamination so that the detrimental effect of airborne contaminants as well as the seeding particles on the surface tension is minimized.

The test section consists of a hollow cylinder made of copper, an insulated bottom made of Teflon®, a wire heater placed at the center axis of the cylindrical container, and a cooling loop to keep the test section wall at a constant temperature. The heater to test section diameter ratio of 10% is maintained for all of the test sections. The Teflon bottom is slideable inside the hollow copper cylinder so that the aspect ratio can be varied. A hollow copper tubing wrapped in a tight coil and soldered to the outside of the copper cylinder forms the cooling jacket for the test sections of diameters 0.96 cm and greater. For the test sections with diameters less than 0.96 cm the sidewalls are in direct contact with running water, as described by Kamotani et al.[6]

Cartridge heaters and nichrome wires of various diameters connected to a dc power supply form the heating system for the range of test sections in this study. The temperature of the heater is controlled by varying the output voltage of the dc power supply.

A Polyscience digital temperature bath (model 9001) using distilled water as the cooling medium is hooked to the cold wall circulation mechanism to form the cooling system. The cooling system temperature is maintained near room temperature (~25°C) to avoid moisture condensation on the test section and thereby to eliminate the possibility of water mixing with the test fluid.

Copper–constantan thermocouples (T type) are used in the experiment because of their sensitivity and fast response time.

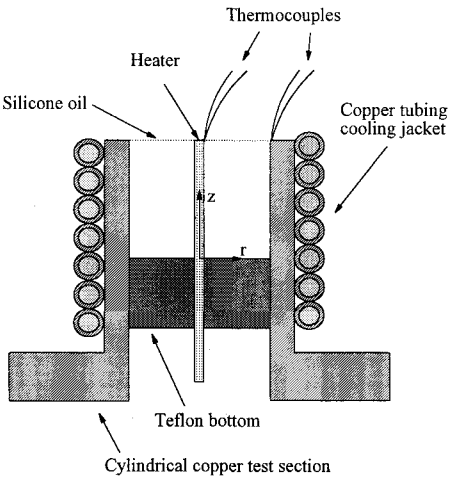

Fig. 1 Cross-sectional view of test section.

A 0.025-mm-diam thermocouple is fixed on the heater by a high temperature and high thermal conductivity adhesive compound for the heater temperature measurement. The size of the thermocouple is chosen so as to minimize disturbances to the flow near the heater. The thermocouple location is adjusted so that its junction is just below the fluid surface to measure the heater temperature close to the liquid free surface.

To monitor the cold wall temperature, a 0.076-mm-diam thermocouple is fixed to the cold wall with the high thermal conductivity adhesive compound at the location shown in Fig. 1. Another 0.076-mm-diam thermocouple (0.025 mm for the test sections smaller than 9.6 mm in diameter) is attached to a *XYZ* positioner and is used for measuring the fluid temperature at various locations. The 0.025- and 0.076-mm thermocouples have a response time of less than 0.02 s in air (faster in liquid), which is sufficient for the temperature oscillation frequency expected in the current experiment (0–4 Hz).

The heater, cold wall, and fluid temperature measuring thermocouples are connected to a Keithly Metrabyte DAS 1600 data acquisition card via an interface. The DAS 1600 card is installed in a 386 personal computer having the Labtech Notebook software for monitoring and recording the temperature data.

Flow visualization is done with a stereo microscope with variable magnification (10–60×) and a long working distance (~5 cm for 60×). A Panasonic WV-5000 high-resolution digital video camera connected to a Panasonic AG-7400 super VHS recorder is also used for this purpose.

An IR imager (Inframetrics model 600) is used to scan the liquid free surface. The imager system was also used in our earlier work[6] and is described in detail by Pline.[18] In the present study the information is used only to observe the free surface temperature variation qualitatively during oscillations.

In the microgravity experiment on oscillatory thermocapillary flow, called the OTFE, it was intended to study the oscillation phenomenon in the present test configuration with container diameters of 1 and 3 cm and with 2- and 5-cS silicone oils.[17] However, bubbles appeared in all of the tests and, unlike in 1-*g* tests where the bubbles rise and escape from the fluid, they stayed in the fluid and grew. They eventually disrupted the flow appreciably, at which point the test had to be stopped. Bubbles were present from the beginning in the 1-cm containers. However, they appeared only at some ΔT in the 3-cm containers and the flow was steady and axisymmetric before the bubble appearance.

Parametric Ranges

The important dimensionless parameters for steady thermocapillary flow in a cylindrical container in the presence of buoyancy are $R\sigma$, Gr, Pr, Ar, and Hr. The Marangoni number

$Ma = R\sigma Pr$ is also used. The ratio of buoyancy to thermocapillary forces is represented by the dynamic Bond number that depends on $R\sigma$ and Gr. According to Ostrach,[19] if the flow is of boundary-layer type, $Bd = Gr/R\sigma^{4/3}$ for a given Ar. According to Kamotani et al.,[20] the flow in the present configuration with a high Pr fluid is of boundary-layer type if $R\sigma > 1000$.

The parametric ranges of the present experiment near the onset of oscillations are $Pr = 10-25$, $R\sigma = 2.3 \times 10^3-1.1 \times 10^5$, $Ma = 4.7 \times 10^4-1.8 \times 10^6$, and $Gr = 1.1 \times 10^3-3.4 \times 10^6$. The physical properties of the fluids are evaluated at the mean temperature of the heater and the sidewall. Since $R\sigma$ is larger than 1000 in all cases, the flow is of boundary-layer type near the onset of oscillations, and the range of the dynamic Bond number is $Bd = 0.03-0.63$.

Experimental Procedure

The experiment is performed as follows:

1) Move the Teflon bottom to obtain the desired aspect ratio.

2) Place the test section on its adjustable platform and make it level horizontally.

3) Align the heater so that it is at the center of the test section.

4) Attach the heater thermocouple to the heater.

5) Clean the test section with alcohol and cotton then blow dry using high-pressure air.

6) Put some barrier coating (Scotchguard®) on the upper surface of the cold wall to pin the silicone oil at the cold wall edge; let dry for at least 45 min.

7) Adjust the light source, video system, and microscope.

8) Fill the test section with the test fluid until the free surface is at the same height as the top of the test section; add the tracer particles.

9) Increase the power to the heater stepwise.

10) Observe the change in the flow structure (the onset of oscillations) by flow visualization.

Experimental Accuracy

The error involved in the measurement of ΔT, including the thermocouple measurement and the data acquisition, is estimated to be within about 5%. The value of ΔT_{cr} is repeatable within the previous accuracy. In the case of small containers ($D < 7$ mm) with thin heating wires, the heater temperature relative to the sidewall temperature varies about 10% along the length, as described by Kamotani et al.[6] For that reason the heater temperature is measured close to the free surface because thermocapillary flow is driven by the temperature gradient at the free surface. The reproducibility in the frequency measurement is 5% for $D < 1.5$ cm and 10% for $D > 1.5$ cm.

Results and Discussion

Basic Flowfield

The basic steady flowfields are discussed first based on the flow visualization and numerical analysis. The numerical analysis is done only for steady flow and is based on the SIMPLER algorithm.[21] The same numerical program has been used in our past work on thermocapillary flow.[6,22,23] The free surface is assumed to be flat and nondeformable and the fluid viscosity varies with temperature. Both the heater and sidewall are kept at uniform temperatures and the bottom wall is assumed to be thermally insulated. The analysis takes into account the heat loss from the free surface through radiation and the forced convection of air induced by the free surface motion. The velocity and stream function are nondimensionalized by $\sigma_T \Delta T/\mu$ and $\sigma_T \Delta T/\mu R^2$, respectively, and the temperature is made dimensionless as $(T - T_C)/\Delta T$. Steady thermocapillary flow in the same configuration as the present one was investigated in detail in the surface tension driven convection experiment (STDCE), conducted aboard the Spacelab in conjunction with the OTFE, and the numerical program was validated by the STDCE data.[22,23] A nonuniform grid is employed with meshes graded toward the hot and cold walls and toward the free surface. In the present configuration an accurate resolution of the surface velocity distribution near the heater is the most important requirement for the numerical grid.[22] Of the various numerical results utilized in this article the largest Ma is 5.6×10^5 with $Bd = 0.52$, $Pr = 21$, and $Ar = 2$. The computed maximum surface velocities for the case with three different grids, 50×60 ($r \times z$), 60×70, and 65×75, with the smallest radial mesh sizes next to the heater being 0.0008, 0.0002, and 0.0001, respectively, are 0.0316, 0.0358, and 0.0364, respectively, and the maximum stream functions are 5.32×10^{-4}, 5.36×10^{-4}, and 5.36×10^{-4}, respectively. Therefore, the 60×70 grid is used for all of the cases presented herein.

Some computed streamlines and isotherms are presented in Fig. 2. The primary flow is a rapid outward flow from the heater to the cold wall along the free surface (called the surface flow) and a return flow is generated in the bulk toward the heater. This flow forms a cell and is termed herein as the primary cell. Pure thermocapillary flow in the present configuration with $Ar = 1$ consists only of the primary cell.[22,23]

Figure 2a shows the computed streamlines for $D = 0.96$ cm for the preoscillatory conditions with and without buoyancy. As seen in the figure, a typical thermocapillary flow pattern prevails over most of the primary cell, even when buoyancy is added. Although Bd is less than unity (0.2), meaning that thermocapillarity dominates over buoyancy, the effect of thermocapillarity decreases away from the free surface so that buoyancy eventually becomes dominant below a certain depth, where, however, the flow is relatively weak. Buoyancy extends a very weak return flow region to a greater depth as seen in Fig. 2a. The computed dimensionless average velocity over the free surface is 10% larger with buoyancy and the difference is reduced to 4% for $Ar = 1$. For the smallest container in the present experiment ($D = 0.39$ cm) the increase in the average

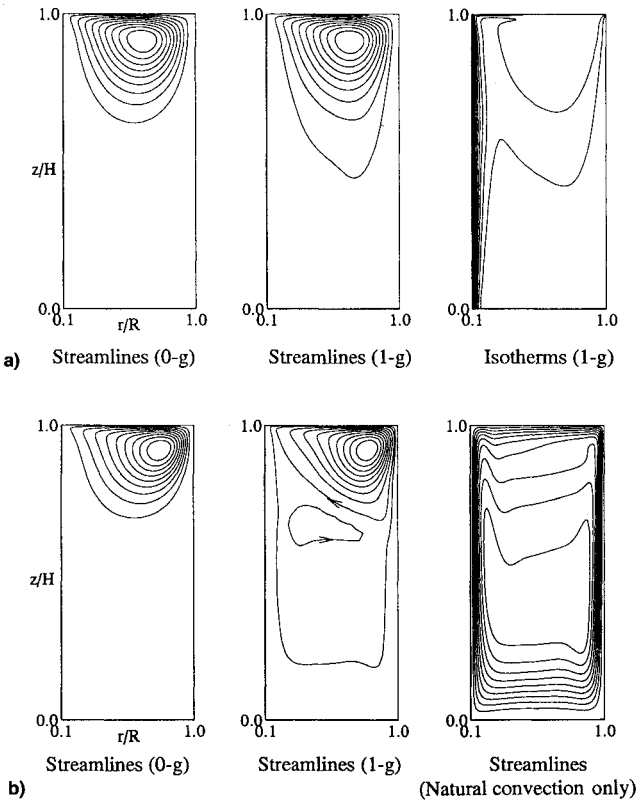

Fig. 2 Computed streamlines and isotherms for 1 and 0 g: a) $D = 0.96$ cm, $Ar = 2.0$, $Ma = 8 \times 10^4$, $Bd = 0.2$, and $Pr = 25$; and b) $D = 2.2$ cm, $Ar = 2.0$, $Ma = 6 \times 10^5$, $Bd = 0.52$, and $Pr = 21$.

surface velocity due to buoyancy is 5% at the conditions of $Ma = 4.5 \times 10^4$, $Pr = 23$, $Ar = 2$, and $Bd = 0.04$. Therefore, although the effect of buoyancy is not negligible on the whole flow, the main flow (the primary cell) is not much influenced by buoyancy in the present tests with diameters less than 1 cm. The isotherms given in Fig. 2a show that most of the temperature variation in the fluid occurs in a relatively small region near the heater. As the heater is relatively small compared to the container radius in the present experiment, the fluid temperature decreases sharply near the heater and is relatively uniform over most of the test section, which tends to minimize the effect of buoyancy on the thermocapillary flow.

As for the effect of Ar on the flow and temperature fields, since the fluid is heated all along the heater, the overall temperature of the primary cell decreases as the heater length is reduced with decreasing Ar. For the conditions of Fig. 2a, the average dimensionless free surface temperature is reduced by 5% of ΔT when Ar is changed from 2 to 1, while the reduction is 1% of ΔT in 0 g. The average surface velocity is reduced by 10% when we change Ar from 2 to 1, partly because natural convection along the heater is reduced (the corresponding surface velocity reduction is 3% in 0 g), and partly because of increased effect of the bottom wall. The overall structure of the primary cell does not change much (e.g., the cell center remains unchanged) when Ar is changed from 2 to 1, except for the weak return flow near the bottom edge of the cell.

The computed streamlines for $D = 2.2$ cm are shown in Fig. 2b. The results obtained without buoyancy or thermocapillarity are also presented here for comparison. As the figure shows, the main flow structure in 1 g is much closer to that of pure thermocapillary flow than to that of pure buoyancy flow, despite the fact that Bd is 0.52. However, the flow in the primary cell is influenced by buoyancy: the average surface velocity is increased by 18% and the average free surface temperature is increased by 10% of ΔT by buoyancy. A close examination of the computed streamlines in 1 and 0 g in Fig. 2b shows that the primary cell is distorted by buoyancy and the main activity in the primary cell shifts toward the cold wall. Flow visualization shows that the flow near the cold wall, which is relatively weak in the small containers, becomes fairly noticeable. Therefore, the overall effect of buoyancy is strong in this case. The motion of the fluid below the primary cell is much weaker, but one clearly visible motion occurs in a small cell just below the primary cell. The flow in the small cell is counterclockwise in Fig. 2b and is generated by the shear force at the edge of the primary cell. When Ar is changed from 2 to 1 in the analysis for $D = 2.2$ cm, the average surface velocity decreases by 14% and the average surface temperature decreases by 5% of ΔT, but the shape of the primary cell does not vary appreciably except for the disappearance of the weak secondary cell.

The preoscillatory flow for $D = 3.1$ cm (the largest diameter in the present experiment) is basically similar to that for $D = 2.2$ cm, except in the former case that the primary cell is more squeezed toward the cold wall by buoyancy and the flow near the cold wall is more active. Therefore, in all of the present tests there exists a cellular motion near the free surface and thermocapillarity is always important. The main effect of buoyancy, if important, is to squeeze the primary cell toward the cold wall.

Oscillatory Flow

If ΔT is increased beyond a certain value (called the critical temperature difference), the flow suddenly becomes three dimensional and time periodic. The oscillatory motion is generally similar to the one described by Kamotani et al.[6] for negligible buoyancy conditions; the fluid particles move back and forth in the azimuthal direction with the frequency of oscillations as they circulate in the primary cell. One noticeable feature in the large containers is that the flow along the cold wall becomes alternately strong and weak, which results in alternately deep and shallow penetration of the flow into the relatively quiescent fluid below the primary cell. By observing the light reflection from the free surface during oscillations one can see that the free surface is in periodic motion when the container diameter is less than about 1 cm. Such free surface motion has been investigated in detail by Lin et al.[24] in the present configuration. For larger containers the surface deformation becomes smaller with increasing diameter as gravity tends to suppress the free surface motion as the static Bond number ($\rho g R^2/\sigma$) increases.

Figure 3 shows the variation of the critical temperature difference ΔT_{cr} with the container aspect ratio for two different container diameters. For the 0.96-cm container, ΔT_{cr} does not vary with Ar except when Ar is below $Ar = 1$. The retardation of the primary cell by the bottom wall becomes important below $Ar = 1$. It is noted that if buoyancy is important in the 0.96-cm container tests, ΔT_{cr} should change with Ar because the natural convection changes as the depth changes. Masud et al.[16] also conducted tests with the 0.96-cm container in which they changed buoyancy by varying the heater length while keeping the fluid depth fixed and showed that ΔT_{cr} did not change with the heater length. Those two facts suggest clearly that the effect of buoyancy on the oscillation phenomenon is not important in the 0.96-cm container. The variation of ΔT_{cr} with Ar for the 2.2-cm test section is not noticeable in the given Ar range (0.75–2.0), which seems to be consistent with the previous numerical result that the primary cell shape does not change with Ar. However, as shown in the numerical analysis, the primary cell is affected by buoyancy. Masud et al.[16] changed the heater length in the 2.2-cm container and showed that ΔT_{cr} was influenced by the heater length. Therefore, the effect of buoyancy on the onset of oscillations is important in the 2.2-cm container. The data presented next are mainly for $Ar = 2$, to eliminate the effect of Ar for all cases. Because of the fact that the total fluid depth does not have strong influence on the oscillation phenomenon in the parametric ranges of the present experiment, the dimensionless parameters Ma and Gr do not contain the depth in the present work.

The values of ΔT_{cr} and the oscillation frequencies for various size test sections are presented in Fig. 4. The frequency was measured near ΔT_{cr} (within about 10% of ΔT_{cr}). Two trends are noticeable. For D less than about 1.5 cm, ΔT_{cr} generally decreases with D and the oscillation frequency is a strong function of D. For D larger than about 1.5 cm, ΔT_{cr} increases rather sharply with D, but the frequency depends less on D than in the case of smaller diameter. The trend for larger D is clearly related to the effect of buoyancy and the trend for the smaller containers is mainly that of 0 g. It is noted that the heater temperature becomes rather high for the large containers so that evaporation from the free surface becomes a concern.

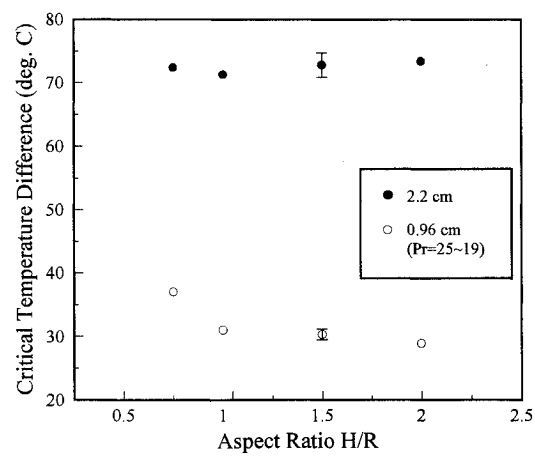

Fig. 3 Variation of critical temperature difference with aspect ratio.

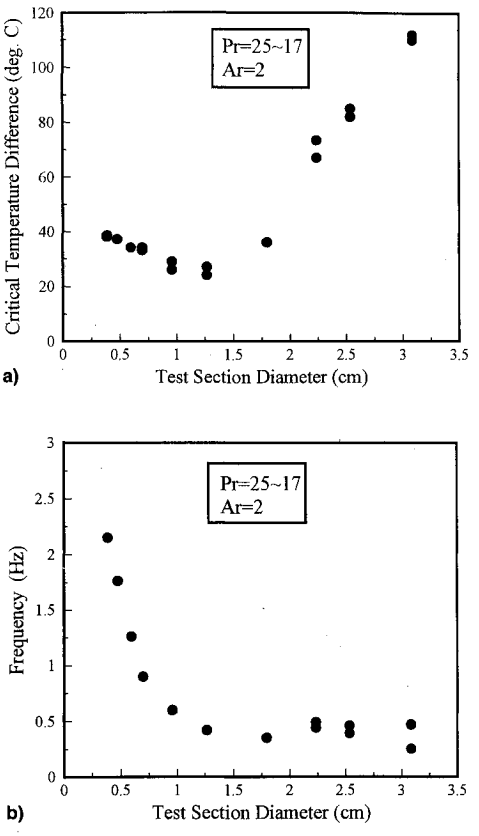

Fig. 4 Variations of a) critical temperature difference and b) oscillation frequency with test section diameter.

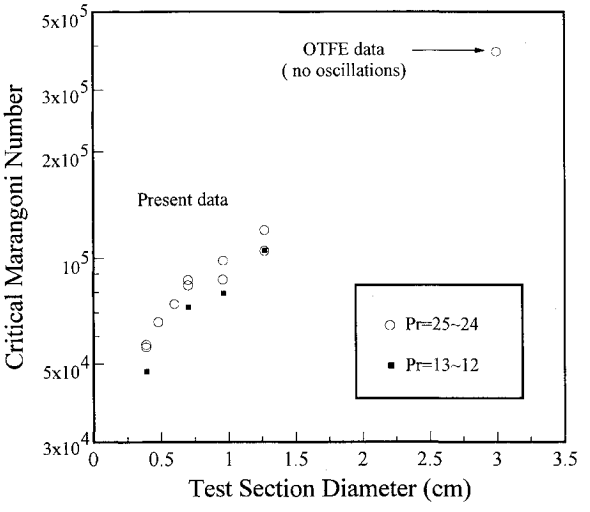

Fig. 5 Critical Marangoni numbers for onset of oscillatory thermocapillary flow.

However, since the fluid temperature decreases very sharply away from the heater as shown earlier, most of the fluid is in a temperature range where the evaporation is not important, as evidenced by the fact that the fluid level is seen to have changed very little during tests with the largest container (D = 3.1 cm).

The data for small containers are analyzed first. If buoyancy and free-surface deformation are negligible, Ma is the only main parameter that contains ΔT, and so ΔT_{cr} is nondimensionalized as Ma_{cr}. In order to show the trend of Ma_{cr}, it is plotted against the dimensional container diameter D in Fig. 5. One data point for D = 3.0 cm with 2-cS silicone oil from the OTFE experiment in microgravity is also shown. The OTFE experiment was interrupted after a bubble appeared in the test cell, but until its appearance the flow was axisymmetric and steady. The value of Ma corresponding to the ΔT just before the interruption is given in Fig. 5 to show that no oscillations were observed at that Ma. As Fig. 5 shows, Ma_{cr} varies with D beyond the experimental error. Including the no-oscillation data of the OTFE, it is clear that Ma_{cr} increases with D. If Ma_{cr} is the only parameter to describe the onset of oscillations, Ma_{cr} should not depend on the dimensional quantity D. Although buoyancy is not completely negligible in the small container tests of the present study, a comparison of the trend of the present data toward smaller D (or toward less buoyancy) and the microgravity data shows clearly that Ma_{cr} changes with D, meaning that Ma is not the proper parameter to specify the onset of oscillations. We are currently working on defining the new parameter for the present experimental configuration.

In the parametric ranges of the present experiment the characteristic velocity of thermocapillary flow is given as $\mu U_{ref}/\sigma_T \Delta T \sim R\sigma^{-1/3}$ according to Ostrach.[19] Since the period of temperature oscillations is considered to scale with the time scale of convection, the dimensionless frequency is given as $f^* = fR/U_{ref} \sim (\mu Rf/\sigma_T \Delta T)R\sigma^{1/3}$. The dimensionless frequencies near the critical conditions are shown in Fig. 6 for $D <$ 1.5 cm. The figure shows that the dimensionless frequency is constant (equal to about 0.03) within the experimental error, which is in agreement with the previous scaling law. The result again proves that the flow and oscillations are mainly driven by thermocapillarity in the small container tests ($D < 1.5$ cm).

Although buoyancy cannot be neglected completely, even in the present small container tests, the fact that the oscillation phenomenon is not influenced appreciably by buoyancy in the range of Bd of those tests is supported by the following result obtained by Schwabe and Scharmann.[25] They investigated oscillatory thermocapillary flow in the float-zone configuration using the same size liquid column (6-mm column of $NaNO_3$) both in 1 g and in microgravity (aboard the Space Shuttle), and found that the onset of oscillations and the oscillation frequency were almost unchanged by the gravity level. In their experiment with column length = 0.48 mm, Bd was 0.3 and 0.3×10^{-5} in 1 g and in microgravity, respectively. That experiment shows that as long as Bd is less than about unity, buoyancy has no influence on the oscillation phenomenon. In comparison, the largest Bd is 0.3 and the smallest is 0.03 in the present small container experiments.

When buoyancy becomes important, the important parameters for the onset of oscillations are Ma and Bd (or Gr) for a given Ar, Hr, and Pr if free-surface deformation is not taken into account. The values of Ma and Bd at the onset of oscil-

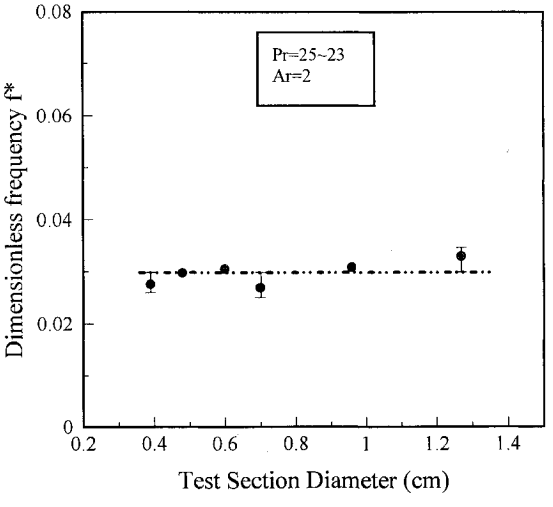

Fig. 6 Dimensionless frequency for oscillatory thermocapillary flow.

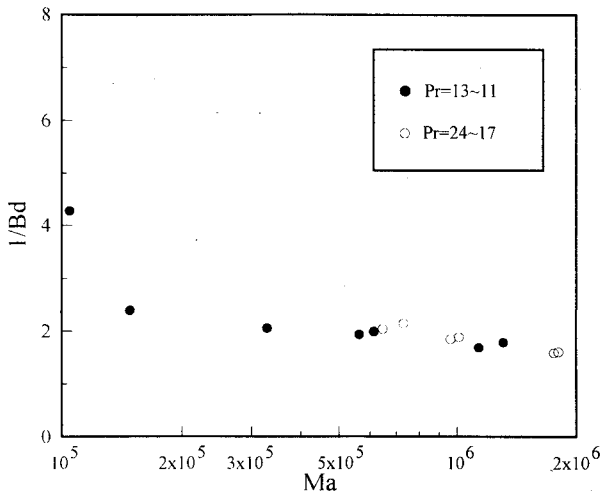

Fig. 7 *Bd* vs *Ma* at onset of oscillations for combined driving force case.

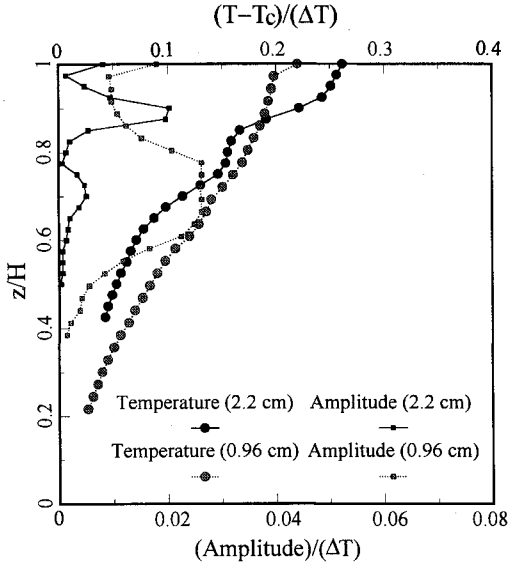

Fig. 8 Distributions of mean temperature and oscillation amplitude for D = 2.2 cm ($Ma = 9.0 \times 10^5$, $Gr = 7.6 \times 10^5$, and Pr = 18.5), and D = 0.96 cm ($Ma = 1.3 \times 10^5$, $Gr = 1.6 \times 10^4$, and Pr = 23.6) at Ar = 2.

lations are plotted in Fig. 7 for large containers ($D \geq 1$ cm). Figure 7 suggests that for D larger than about 1.5 cm ($Ma > 2 \times 10^5$), the flow becomes oscillatory when Bd^{-1} becomes larger than a certain value (about 2.0). That result shows that 1) both thermocapillarity and buoyancy are involved in the oscillation mechanism and 2) their ratio (thermocapillarity/buoyancy) must be larger than a certain value for the oscillations to occur. For the onset of oscillations the critical ΔT_{cr} increases very sharply with D (proportional to D^5 for a given Ar), so that in practice oscillatory thermocapillary convection with buoyancy occurs under rather limited diameter ranges in the present configuration.

The frequency of oscillations in the large container tests is roughly constant, independent of D, for a given Pr as shown in Fig. 4, but the data tends to scatter near the largest diameter due to the appearance of different oscillation patterns near the onset of oscillations, as will be discussed later. Since the velocity scale cannot be easily determined when both driving forces are involved and since the frequency data has the earlier scatter, we will not attempt to nondimensionalize the frequency for the large container tests.

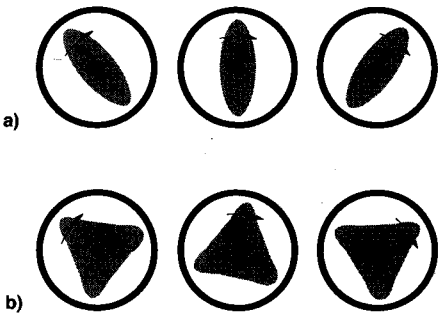

Fig. 9 Sketches of IR images during oscillations: a) two- and b) three-lobed patterns.

The distributions of the mean fluid temperature and the rms temperature fluctuation level (nondimensionalized by ΔT) measured during oscillations are shown in Fig. 8 for two diameters. At this radial location (r/R = 0.5) the highest oscillation amplitude occurs in the interior region, not near the free surface. Comparison of the mean temperature and oscillation amplitude distributions shows that the oscillation level is high in the region where the vertical temperature gradient is large, namely in the interface region between the primary cell and the relatively stagnant region. In the case of D = 2.2 cm there exists a secondary cell (see Fig. 2a), which produces two interfaces where the vertical temperature gradient is large and a relatively uniform temperature region in between as seen in Fig. 8. Therefore, the oscillation amplitude distribution has two peaks in the bulk fluid, the larger one occurring just below the primary cell. In the region closer to the heater the radial temperature gradient near the free surface becomes larger than the vertical gradient in the interior, which causes large temperature fluctuations near the free surface.[6]

The IR image of the free surface is very useful in understanding what is happening during oscillations. In the case of small containers (D < 1.5 cm) an axisymmetric IR image changes to an elliptical pattern after the onset of oscillations and the pattern rotates as illustrated in Fig. 9. The pattern suggests that at a given time the convection along the free surface is strong in two diametrically opposed directions (the elongated directions of the pattern), corresponding to the active period in those directions, and relatively weak (the weak period) in the directions normal to the elongation. Therefore, one rotation of the pattern produces two temperature peaks and valleys at a fixed location. In contrast, in the case of larger containers, especially for the largest container (D = 3.1 cm), the IR image takes various patterns depending on several factors such as ΔT, the past history of heater power variation, outside disturbances, and the slight nonsymmetry of the test configuration. The most noticeable patterns are the previous elliptical pattern and a pattern with three lobes (see Fig. 9). Those patterns generally rotate around the container axis, but sometimes they just change shapes with time without rotating. Because of this pattern shifting, the frequencies of oscillations measured by the thermocouple placed at one location have some scatters.

At this point, an important question to ask is, what physical mechanism is involved in the oscillation phenomenon in the presence of buoyancy. As discussed earlier, the activity near the cold wall is fairly noticeable during oscillations in the large containers. The downward flow along the cold wall becomes strong and weak alternately. When the flow is strong, it penetrates deeper into the quiescent fluid below, but eventually it is pushed up by buoyancy. This interplay between the flow inertia and thermal stratification seems to play an important role in the oscillation mechanism in the large containers, although more work needs to be done to clarify this point.

Conclusions

Oscillatory convection due to combined thermocapillarity and buoyancy is studied experimentally in the present work. Cylindrical containers of various sizes and 1- and 2-cS silicone oils are used. Numerical analysis of steady flows is also conducted to supplement the experiment. It is shown that the critical ΔT and the oscillation frequency exhibit two different trends, one for small containers and the other for large containers. The former trend is shown to be for negligible buoyancy conditions by numerical and scaling analyses. When buoyancy is negligible, the conditions for the onset of oscillations cannot be characterized by the Marangoni number alone. On the other hand, when buoyancy is not negligible, the dynamic Bond number alone specifies the onset conditions.

Acknowledgment

This work is funded by NASA through Grant NAG3-1568 with T. Jacobson of the NASA Lewis Research Center as the Project Manager.

References

[1]Schwabe, D., and Scharmann, A., "Some Evidence for the Existence and Magnitude of a Critical Marangoni Number for the Onset of Oscillatory Flow in Crystal Growth Melts," *Journal of Crystal Growth*, Vol. 46, No. 1, 1979, pp. 125–131.

[2]Chun, C.-H., and Wuest, W., "Experiments on the Transition from Steady to the Oscillatory Marangoni Convection of a Floating Zone Under Reduced Gravity Effect," *Acta Astronautica*, Vol. 6, No. 9, 1979, pp. 1073–1082.

[3]Preisser, F., Schwabe, D., and Scharmann, A., "Steady and Oscillatory Thermocapillary Convection in Liquid Columns with Free Cylindrical Surface," *Journal of Fluid Mechanics*, Vol. 126, Jan. 1983, pp. 545–567.

[4]Kamotani, Y., Ostrach, S., and Vargas, M., "Oscillatory Thermocapillary Convection in a Simulated Floating Zone Configuration," *Journal of Crystal Growth*, Vol. 66, No. 1, 1984, pp. 83–90.

[5]Velten, R., Schwabe, D., and Scharmann, A., "The Periodic Instability of Thermocapillary Convection in Cylindrical Liquid Bridges," *Physics of Fluids A*, Vol. 3, No. 2, 1991, pp. 267–279.

[6]Kamotani, Y., Lee, J. H., Ostrach, S., and Pline, A., "An Experimental Study of Oscillatory Thermocapillary Convection in Cylindrical Containers," *Physics of Fluids A*, Vol. 4, No. 5, 1992, pp. 955–962.

[7]Lee, J. H., Kamotani, Y., and Ostrach, S., "A Study of Thermocapillary Convection in Circular Cylinders with CO_2 Laser Heating," Case Western Reserve Univ., Rept. EMAE/TR-94-213, Cleveland, OH, 1994.

[8]Bergman, T. L., and Ramadhyani, S., "Combined Buoyancy- and Thermocapillary-Driven Convection in Open Square Cavities," *Numerical Heat Transfer*, Vol. 9, No. 4, 1986, pp. 441–451.

[9]Carpenter, B. M., and Homsy, G. M., "Combined Buoyant-Thermocapillary Flow in a Cavity," *Journal of Fluid Mechanics*, Vol. 207, Oct. 1989, pp. 121–132.

[10]Metzger, J., and Schwabe, D., "Coupled Buoyant and Thermocapillary Convection," *Physico-Chemical Hydrodynamics*, Vol. 10, No. 3, 1988, pp. 263–282.

[11]Villers, D., and Platten, J. K., "Separation of Marangoni Convection from Gravitational Convection in Earth Experiments," *Physico-Chemical Hydrodynamics*, Vol. 8, No. 2, 1987, pp. 173–183.

[12]Ben Hadid, H., and Roux, B., "Melt Motion in Differentially Heated Horizontal Cavities: Motion Due to Buoyancy and Thermocapillarity," *Journal of Fluid Mechanics*, Vol. 221, Dec. 1990, pp. 77–103.

[13]Mundrane, M., and Zebib, A., "Oscillatory Buoyant Thermocapillary Flow," *Physics of Fluids*, Vol. 6, No. 10, 1994, pp. 3294–3305.

[14]Villers, D., and Platten, J. K., "Coupled Buoyancy and Marangoni Convection in Acetone: Experiments and Comparison with Numerical Simulations," *Journal of Fluid Mechanics*, Vol. 234, Jan. 1992, pp. 487–510.

[15]Lee, K. J., and Kamotani, Y., "Combined Thermocapillary and Natural Convection in Rectangular Enclosures," *Proceedings of the 3rd ASME/JSME Thermal Engineering Conference* (Reno, NV), Vol. 1, American Society of Mechanical Engineers, New York, 1991, pp. 115–120.

[16]Masud, J., Kamotani, Y., and Ostrach, S., "An Experimental Study of Combined Thermocapillary and Natural Convection in Cylindrical Containers," Case Western Reserve Univ., Rept. EMAE/TR-93-211, Cleveland, OH, 1993.

[17]Kamotani, Y., Ostrach, S., and Pline, A., "Oscillatory Thermocapillary Flow Experiment (OTFE)," NASA CP 3272, Vol. 2, May 1994, pp. 701–715.

[18]Pline, A., "Development of an Infrared Imaging System for the Surface Tension Driven Convection Experiment," NASA TM-101479, Jan. 1989.

[19]Ostrach, S., "Motion Induced by Capillarity," *Physico-Chemical Hydrodynamics*, V. G. Levich Festschrift, Vol. 2, Advanced Publication, 1977, pp. 571–589.

[20]Kamotani, Y., Chang, A., and Ostrach, S., "Effects of Heating Mode on Steady Axisymmetric Thermocapillary Flows in Microgravity," *Heat Transfer in Microgravity*, edited by S. S. Sadhal and A. Gopinath, American Society of Mechanical Engineers HTD-Vol. 290, 1994, pp. 53–62.

[21]Patankar, S. V., *Numerical Heat Transfer and Fluid Flow*, McGraw–Hill, New York, 1980.

[22]Kamotani, Y., Ostrach, S., and Pline, A., "A Thermocapillary Convection Experiment in Microgravity," *Heat Transfer in Microgravity*, edited by C. T. Avedesian and V. A. Arpaci, American Society of Mechanical Engineers HTD-Vol. 269, 1993, pp. 23–30.

[23]Kamotani, Y., Ostrach, S., and Pline, A., "Analysis of Velocity Data Taken in Surface Tension Driven Convection Experiment in Microgravity," *Physics of Fluids*, Vol. 6, No. 11, 1994, pp. 3601–3609.

[24]Lin, J., Kamotani, Y., and Ostrach, S., "An Experimental Study of Free Surface Deformation in Oscillatory Thermocapillary Flow," *Acta Astronautica*, Vol. 35, No. 8, 1995, pp. 525–536.

[25]Schwabe, D., and Scharmann, A., "Measurements of the Critical Marangoni Number of the Laminar-Oscillatory Transition of Thermocapillary Convection in Floating Zones," *Proceedings of the 5th European Symposium on Material Sciences Under Microgravity*, European Space Agency, ESA SP-222, Vol. 1, Nov. 1984, pp. 281–289.